Embedded 3D Printing Based on High Elastomeric Strain Wireless Sensor

Hongwei Wang(✉), Yue Wu, Xiaogang Ren, and Zhiying Cao

The Affiliated Changshu Hospital of Soochow University
(Changshu No.1 People's Hospital), Suzhou 215500, Jiangsu, China
1040558124@qq.com

Abstract. In view of the high degree of personalization of embedded 3D printing products, traditional 3D printing is not applicable. This paper presents an embedded three-dimensional printing technology based on high elastic strain wireless sensor. The whole method framework includes mechanical system, control module and visual module. Firstly, three non-collinear points on the high elastic strain wireless sensor are used to align the guide plate and the model. Then, according to the position and direction of the guide hole on the high elastic strain wireless sensor, the mechanical system is controlled to guide the model guide hole to move to the center of the visual module. The characteristic parameters such as roundness, length-width ratio, diameter and center distance of the guide hole are analyzed to determine whether the guide hole is qualified. The experimental results show that compared with the traditional three-dimensional printer, the three-dimensional printer designed in this paper shortens the production cycle and improves the print resolution.

Keywords: High elastomeric strain · Wireless sensor · Embedded · 3D printing products · Quality manufacturing

1 Introduction

3D printing is an additive manufacturing technology that can be used to quickly complete the industrial design or mold manufacturing. With the rise of this technology, some breakthrough methods can be implemented [1, 2]. Great breakthroughs have been achieved in the major subject of Beijing Municipal Science and Technology Commission "Development and manufacturing of the embedded 3D printing tumor medical guide plate forming equipment and manufacturing equipment engineering prototype" undertaken by Beijing University of Technology [3, 4]. In this treatment method, guide plate model is designed based on the conditions of the patients, and the therapeutic guide plate is generated through the embedded 3D printing technology. The doctor inserts the therapeutic probe along the guide hole on the guide plate into the patient's tumor location to implement the radiotherapy. Hence, the forming of the guide hole has a significant effect on the therapeutic effect [5–7]. However, the forming of the guide hole cannot guarantee the direct use [8, 9], which does not match the rapid development of the 3D printing technology. At present, the embedded 3D printer manufacturing is still in the blank stage and lack of systematic manufacturing means [10].

Y.-D. Zhang et al. (Eds.): ICMTEL 2020, LNICST 327, pp. 422–437, 2020.
https://doi.org/10.1007/978-3-030-51103-6_38

The embedded 3D printing products have very strong personalized features. Take the frontal tumor guide plate in this paper as an example. Each guide plate is designed for the individual patient. The location and orientation of each guide hole will be different from those of the other guide plates. Hence, the assembly line product manufacturing scheme is not applicable to the manufacturing of personalized product based on the embedded 3D printing [11, 12].

In recent years, computer vision technology has developed rapidly, and the vision-based 3D printer manufacturing technology has gradually been developed for the product application. For example, the machine vision system for the red pepper contaminated by aflatoxin, the gilthead freshness intelligent manufacturing system based on machine vision [7], the application of machine vision technology to make tiny cracks on the surface of biscuits. In this scheme, one plane of the object to be tested is fabricated, and the plane to be fabricated for each product is the same, so that the camera and the object to be tested can remain relatively fixed in the locational relationship, which cannot meet the multi-angle manufacturing requirements of embedded 3D printing products. Tile automatic visual quality control intelligent system based on machine vision [11, 12]. Button battery online manufacturing system based on machine vision. These systems are coupled with the conveyor belt to make product manufacturing more automated. It is possible to manufacture multiple products one by one, while still maintaining a relatively static relationship for each product [13]. Hence, it can be seen that the 3D printer manufacturing based on machine vision is currently a research hotspot, but the current manufacturing systems are mostly based on the integration of the computer vision and control modules. The products manufactured are relatively simple, the manufacturing path is fixed, and only one surface is fabricated in most of the products to be tested or the products are fixed so that the part to be tested and the location of the vision system remains unchanged. In this way, it is highly difficult to adapt to the products that are not in the design template. In case of the manufacturing based on the embedded manufacturing 3D by using the traditional quality manufacturing system, it will inevitably result in reduced manufacturing efficiency or even inability to manufacture the printing products due to the high degree of freedom of embedded 3D printing products [14].

In order to solve the above problems, a systematic embedded 3D printer manufacturing framework is put forward in this paper, and a prototype system is developed to verify the principle. The system is based on the model guidance, mechanical system coordination, supplemented by visual monitoring to achieve embedded 3D printer quality manufacturing. The main idea is to make use of the guide plate and corresponding three non-collinear points on the high elastomeric strain wireless sensor to align the coordinates of the guides and the model of the three, and then in accordance with the guide hole, the high elastomeric strain on the triangular surface of the wireless sensor. Subsequently, the geometric feature is used to extract the center coordinate and the normal vector of the guide hole and plans the manufacturing path. Finally, through the image of the guide hole, in accordance with the roundness, length-width ratio, diameter, and pitch of center hold in the guide hole, whether the guide hole is qualified is determined. In the traditional 3D printer, the design method and system put forward in this paper can shorten the manufacturing cycle and improve the printing resolution.

2 High Elastomer Strain Wireless Sensor

High elastomer strain wireless sensor is composed of elastomer and resistance strain gauge. Elastomer is the basis of high precision force sensor. Strain gauge is the core of sensor elastomer has many forms and complex structure. To design high precision force sensor, the geometry and material of elastomer must be reasonably selected and designed according to its range and accuracy. The guiding principle of designing high precision force transducer is to pursue good natural linearity, improve the output sensitivity of the transducer, and make the transducer have strong lateral resistance. At the same time, the transducer has simple structure, easy sealing, easy processing and so on.

Like other strain elastomers, the working principle of double-circular-hole beam elastomer is based on the deformation principle of metal elastomer and the strain principle of resistance strain gauge, that is, the physical phenomenon that resistance strain gauge changes resistance value with the deformation of elastomer under the action of external weight and force, resistance strain gauge is firmly bonded to the elastic surface of double-circular-hole beam with thermosetting resin binder. Four resistance strain gauges are connected to the Whiston bridge circuit. before the external force acts, the bridge is pre-balanced under the external force, the resistance strain gauge changes with the deformation of the elastomer with double circular holes, so that the strain bridge produces a voltage output signal proportional to the weight or external force.

According to Hooke's law, within the limit range of elasticity, the deformation of an elastic body is proportional to the stress, that is, to the force it is subjected to:

$$\varepsilon = \frac{\sigma}{E} \tag{1}$$

In the formula, ε represents the deformation of an elastic body. E represents the stress of an elastomer. σ represents Young's modulus of elastomeric materials

When the resistance strain gauge deforms with the deformation of the elastomer, the resistance strain gauge changes its geometric size and physical properties, thereby changing the resistance value:

$$\frac{\Delta R}{R} \Big/ \frac{\Delta I}{I} = K = I + 2M + \frac{\Delta P}{p} \Big/ \frac{\Delta I}{I}$$

$$\Delta R = kR\varepsilon = \frac{kR\sigma}{E} \tag{2}$$

In this formula, $\Delta R/R$ represents the relative resistance change of the resistance strain gauge. R represents Poisson's ratio of foil for resistance strain gauge. K represents the sensitivity of resistance strain gauge. P represents resistivity of Strain Resistance Materials.

The elastomer structure of the sensor is shown in Fig. 1. It is a double-circular-hole double-beam with one fixed end and one stressed at the other end. The double-beam is

processed from the whole material, so the structure is very stable and reliable. When the external force or weight acts on the elastomer of the double-circular-hole beam, it will deform. In order to simplify the calculation of the sensor, the double-circular-hole double-beam can be simplified as one fixed end and the other end only along the force side. For statically indeterminate rectangular double beams which move towards the direction but cannot rotate, the combined calculation method should be used in the calculation.

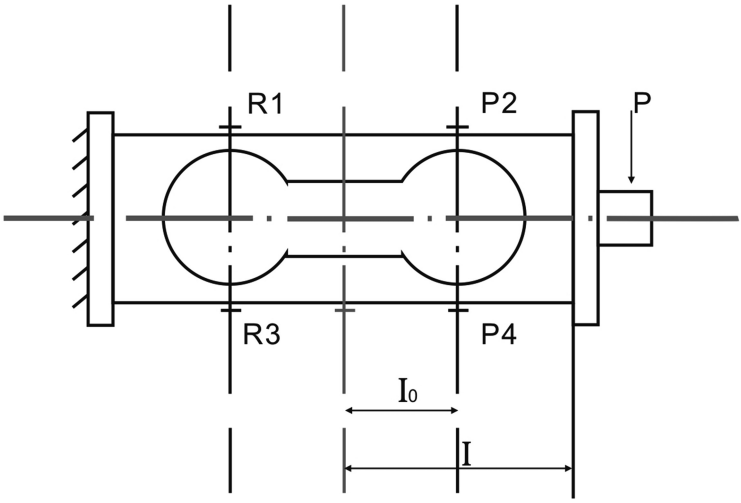

Fig. 1. Double circular holes and double beams

3 Overall Design Framework of the Embedded 3D Printing System

The embedded 3D printer quality manufacturing in this paper is used for the quality manufacturing of the guide hole shape. Its nature is the consistent manufacturing of the high elastomeric strain wireless sensor and the product. The machine vision method is a relatively efficient method, and the installation is simple, with relatively low cost. However, the traditional machine vision method cannot complete the manufacturing of the guide holes with different orientations in the direction of the guide plates. To address this issue, this paper put forward a method to guide the calculation of manufacturing paths through high elastomeric strain wireless sensors, in which the mechanical system coordinates with the machine vision to establish the shape and quality manufacturing framework of the embedded 3D printing product for the product location and quality manufacturing. The overall framework of the system is shown in Fig. 2 as the following.

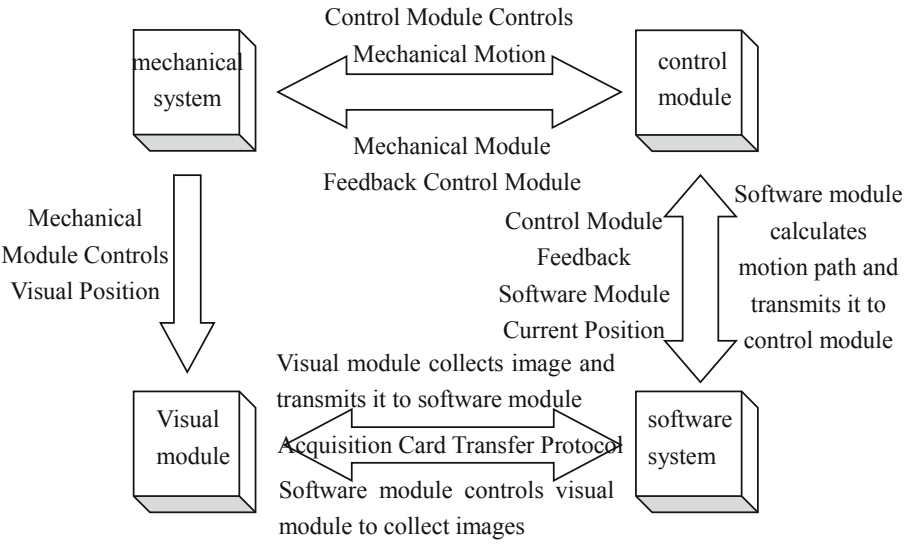

Fig. 2. Overall framework of the system

In the above figure, the software module is used to analyze the high elastomeric strain wireless sensor to calculate the motion path, so that the orientation of the guide hole can be parallel to the optical axis of the camera. In addition, it is located at the center of the camera, and then transmits the motion path to the control module, and the control module transmits a signal to the mechanical module motor, which controls the movement of the mechanical module. The location of the vision module relative to the guide is changed accordingly. At this point, the software module can be used to control the vision module to collect images and feed back to the software module. After the motion is in place, the mechanical module sends the feedback signal to the control module, and the control module gives feedback on the current mechanical module location of the software module in accordance with the signal.

4 Hardware Design of the Embedded 3D Printer System

The embedded 3D printer system hardware system is mainly responsible for the image acquisition and transmission, the guide plate location and camera location movement, the current location information reading and so on. In accordance with the above tasks, the hardware system structure designed in this paper is shown in Fig. 3 as the following. The hardware system mainly includes the mechanical structure and the electric control system.

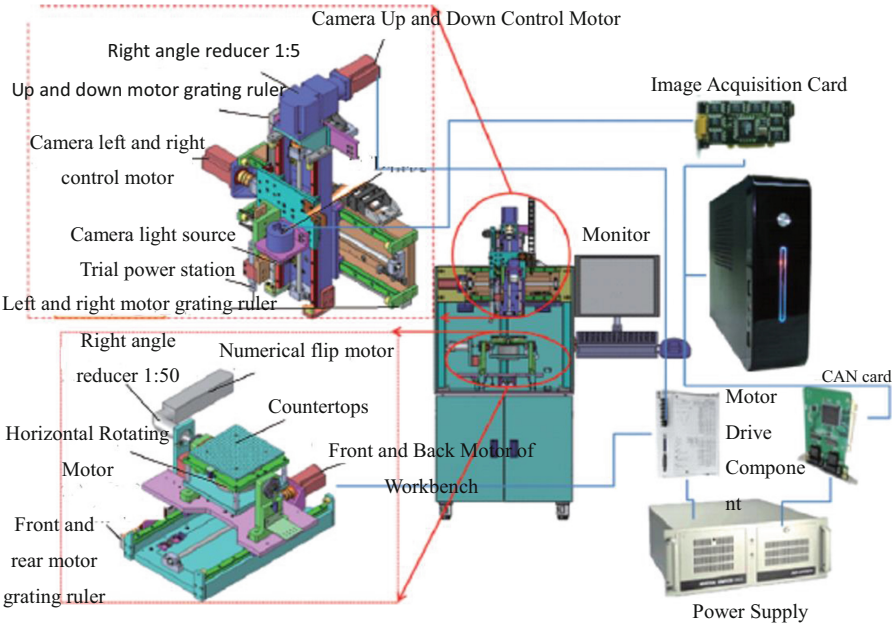

Fig. 3. Hardware system of the system

4.1 Mechanical Structure of the Embedded 3D Printing

The embedded 3D printing model can be simplified into a hemisphere. In this way, the guide hole is inserted on the hemisphere. In order to move the guide hole to the center of the camera and the orientation being parallel to the optical axis of the camera, the design based on the principle of the five-axis digital control machine tool includes two rotating shafts, θ_1 and θ_2, and a mechanical system with three translational axes, xyz, in which a single industrial camera is mounted on the y axis to form a CCD manufacturing mechanism with the x axis; θ_1 and θ_2 are mounted on the z axis, where θ_1 can drive the rotation of θ_2, and the above three constitute a three-dimensional work desk.

4.2 Electric Control System of the Embedded 3D Printing

The embedded 3D printing based on model guidance and visual monitoring the front surface of the tumor guide intelligent quality manufacturing system electrical system is mainly composed of the upper computer, motor control components, image acquisition equipment. The upper computer uses a general-purpose PC, which runs the self-programmed embedded 3D printing frontal surface tumor guide intelligent quality manufacturing software in the win7 system. The motor control component is based on the CAN protocol communication industrial computer. The CAN card adopts the CAN-PCI-02 by copley. The image acquisition equipment adopts the Siliconsoftware_mico-renableiv_vd4-cl image acquisition card, and the camera used is the SP2000 HD camera.

5 Quality Design Method for the Embedded 3D Printer

Combined with the mechanical system, the framework of the guide plate quality design method is shown in Fig. 4 as the following. The design method can mainly be divided into the following three parts:

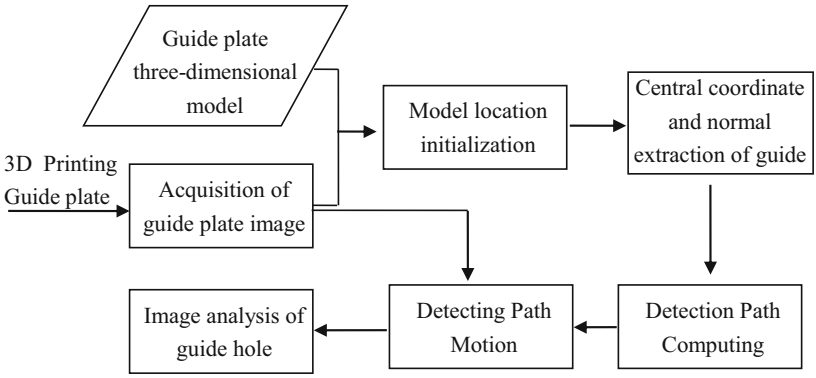

Fig. 4. Framework of the quality design methodology

(1) Initialization of the model location. In order to ensure that the model is consistent with the product, we must first ensure that the model coordinates and the guide coordinates are consistent. Hence, it is required to initialize the model location to align the high elastomeric strain wireless sensor coordinates of the guide with the world coordinates of the guide plate.
(2) Computation of the guide hole path. Each embedded 3D printing product has a corresponding model, which is the advantage of the embedded 3D printing products. It is possible to pre-estimate the location of the target to be tested through the model to determine the manufacturing path. This is efficient and convenient to manufacture by computer vision technology alone, which is also the significance of the model guidance put forward in this paper.
(3) 3D printer manufacturing. After the guide hole is moved to the location to be tested, the quality manufacturing is carried out by means of the images.

For an embedded 3D printed tumor guide to be manufactured, the guide points and the three approximate points on the model are first selected. In accordance with the high elastomeric strain wireless sensor, the world coordinates of the three points on the guide plate under the mechanical system are identified, and then the transformation matrix in the process of converting the model coordinates to the world coordinates of the guide plate is obtained. Subsequently, the other points of the guide are aligned with the process transformation to complete the model coordinates and the world coordinates of the guide plate. Then, the center coordinate and the normal vector of the guide hole cross section in the guide model are extracted and converted into the mechanical path recognizable motion path. The Dijkstra design method is used for optimization to control machinery system movement in the manufacturing path.

In this way, a guide hole can move to the location to be tested and stop, where the images are collected and analyzed to correct the location of the guide hole so that the center of the guide hole is located at the center of the image. Finally, the contour roundness, length-width ratio, diameter, distance from the previous hole and other information of the guide hole is determined to determine whether the pilot hole is qualified.

5.1 Location Initialization of the Embedded 3D Printer Model Based on the High Elastomeric Strain Wireless Sensor

In normal cases, the model of embedded 3D printing is obtained by high elastomeric strain wireless sensor editing software design or scanned by 3D scanner. Hence, each model can be considered as unconstrained from the coordinates of each vertex except for special requirements. In the embedded 3D printer of this paper, the locations and directions of different models in the same coordinate system are very different. In this way, a single matrix transformation formula can be used to align the high elastomeric strain wireless sensor with the physical location is impossible. If three non-collinear points on one object are known, the attitude of the object can be basically determined. In this paper, the world coordinates of the three non-collinear points of the guide are determined through the high elastomeric strain wireless sensor [9] and the corresponding points on the high elastomeric strain wireless sensor are picked up by the mouse, which are converted to the world coordinates in accordance with the calculation formula of binocular stereoscopic image. In combination with the mechanical structure, the world coordinate calculation formula of the marker point is deducted as the following.

$$\begin{bmatrix} x_w \\ y_w \\ z_w \\ 1 \end{bmatrix} = \begin{bmatrix} 1 & 0 & 0 & -c_x \\ 0 & 0 & -1 & c_y - D \\ 0 & 1 & 0 & -c_z \\ 0 & 0 & 0 & 1 \end{bmatrix} \begin{bmatrix} \frac{ft_x - X_r t_z}{f(X_r - X_1)} X_1 \\ \frac{ft_x - X_r t_z}{f(X_r - X_1)} Y_1 \\ \frac{ft_x - X_r t_z}{X_r - X_1} \\ 1 \end{bmatrix} \tag{3}$$

In the above equation: x_w, y_w and z_w stand for the world coordinate of the mechanical system lower guide mark; c_x, c_y and c_z stand for the mechanical system horizontal rotation center, which are the coordinates of the camera coordinate system where the image center is located; D stands for the distance from the horizontal rotation center to the front and back flip center; f stands for the camera focal length. The points on the model are shifted to the location of the actual world coordinate of the guide. Firstly, the 3 points on the model are rotated in accordance with the rotation in any space in the space, and then the triangle formed by the 3 points on the model is rotated to the corresponding edge of the triangle formed by the three points on the guide plate. Finally, the three points on the model are translated to the approximate locations of the three points on the guide plate. In accordance with this transformation process, the other points of the model are transformed to align the guide plate model with the actual location of the guide plate.

5.2 3D Printer Manufacturing and Path

5.2.1 Design Method for the Three-Dimensional Coordinate and Normal Vector Extraction of the Guide Hole

In this paper, quality manufacturing of the guide holes based on the embedded 3D printer is mainly carried out. Each guide plate corresponds to two high elastomeric strain wireless sensors. One is the embedded 3D3D printer model, and the other is the matching guide pin model. Based on the characteristics of the high elastomeric strain wireless sensor STL, the model is formed by a triangular face, and the three vertex coordinates and the normal vector of each triangular face are known. By extracting the triangular faces of the end faces of the guide holes manually, the geometric features of the triangular face and other triangular faces are identified accordingly. Hence, the three-dimensional coordinate and normal vector extraction design method of the guide hole based on geometric feature filtering and clustering is adopted as the following.

Firstly, based on the length and area of the triangular face, the triangular faces of the guide pin model that do not conform to the cross-section features of the guide holes are filtered out, and then the K-means cluster design method is adopted to cluster in accordance with the normal vector to obtain the triangular face sets in the same direction. The K-means clustering of the inner centroid of the triangle is performed inside the set, and each set of triangular faces which may be the cross section of the guide hole is segmented, and the central coordinates and normal vectors of each set are obtained. The guide plate model is estimated by a set of central coordinates and normal vectors. The location of the guide hole in the cross section, only the triangular face at the estimated location is used for the next calculation. Subsequently, the discrete curvature of the remaining triangular faces is calculated by the triangular mesh vertices discrete curvature calculation method based on the Voronoi diagram as the following.

$$K = \frac{2\pi - \sum \theta_i}{S} \tag{4}$$

In the above equation: K stands for the discrete curvature of V_0; θ_i stands for the angle between V_0 and V_{i+1}; S stands for the area of the triangle containing V_0.

In the experiment, if the discrete curvatures of the three vertices of the triangle are two positive and one negative, it is considered to be the required triangle, and vice versa. The calculation model is shown in Fig. 5 as the following.

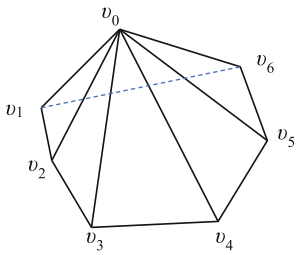

Fig. 5. Discrete curvature calculation model

The triangular surface after filtering is projected along a normal vector to a plane, and is made a circle by Hough transform. If it is a circle, it is considered to be a guide hole cross section. In accordance with the coordinates of the triangular surface in the three-dimensional coordinate system, the polygon center can be obtained. The method is used to obtain the center of the circle, and the average of the triangular surface normal vector is used as the normal vector of the cross section of the guide hole; otherwise, it is not considered to be the guide hole cross section.

5.2.2 3D Printer Manufacturing Path Calculation and Planning

As the mechanical motion cannot directly move in accordance with the coordinates and the normal vector, it is required to plan a path corresponding to the path of the mechanical device in accordance with the extracted guide hole coordinates and the normal vector. The purpose of the motion is to make the guide hole face the guide hole normal vector vertically to the camera plane. In addition, the center of the guide hole is at the center of the image, as shown in Fig. 6 as the following.

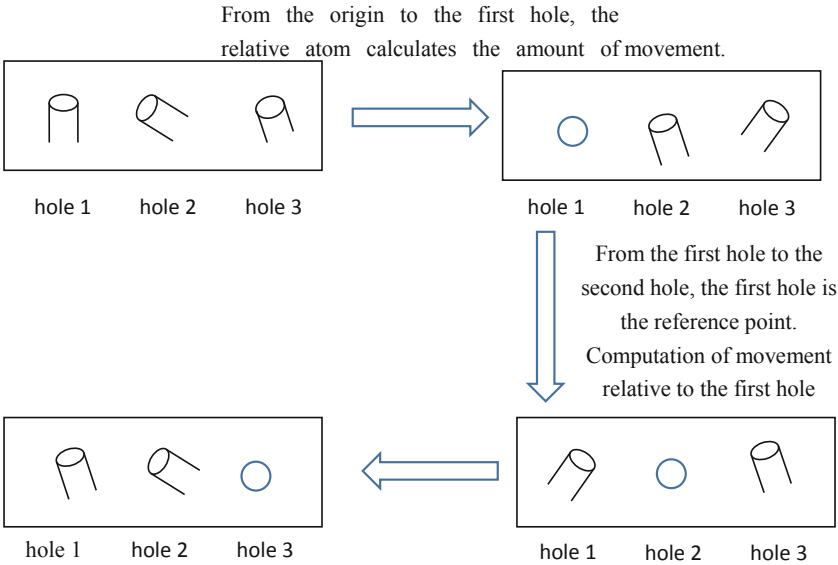

Fig. 6. Schematic diagrams of the guide hole in place

Firstly, the center coordinates of the similar normal vectors are grouped into one group. Subsequently, starting from the three-dimensional rotation matrix, the normal vector is decomposed to identify how the normal vector can be parallel to the y axis by the rotation of the y axis and the x axis, as shown in Fig. 7 as the following.

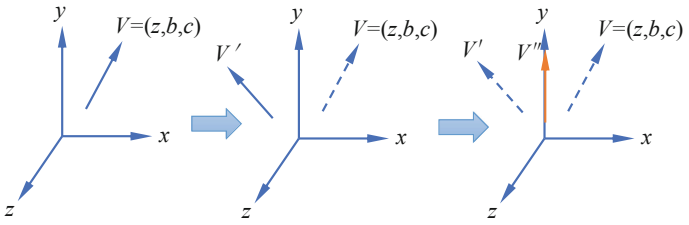

Fig. 7. Schematic diagram of the normal vector rotation

Two rotation angles α and β are as the following

$$\begin{cases} \beta = arccos \frac{c}{\sqrt{a^2 + c^2}} \\ \alpha = arccos \frac{b}{\sqrt{a^2 + b^2 + c^2}} \end{cases} \tag{5}$$

In accordance with the rotation angle, the coordinates of each point in the group after the rotation can be obtained as the following.

$$\begin{bmatrix} x' \\ y' \\ z' \\ 1 \end{bmatrix} = \begin{bmatrix} cos\,\beta & 0 & -sin\,\beta & 0 \\ 0 & 1 & 0 & 0 \\ sin\,\beta & 0 & cos\,\beta & 0 \\ 0 & 0 & 0 & 1 \end{bmatrix} \cdot \begin{bmatrix} 1 & 0 & 0 & 0 \\ 0 & cos\,\alpha & sin\,\alpha & 0 \\ 0 & -sin\,\alpha & cos\,\alpha & 0 \\ 0 & 0 & 0 & 1 \end{bmatrix} \begin{bmatrix} x \\ y \\ z \\ 1 \end{bmatrix} \tag{6}$$

Finally, the path is planned in accordance with the design method to obtain the translation path. The aforementioned process is repeated to traverse each hole, and the angle of rotation and the distance of translation constitute the motion path of the mechanical system accordingly.

6 Experiment and Result Analysis

At present, there is no unified international standard for evaluating the quality of 3D printing. In addition to the control system designed in this paper, the print quality of the STL model is also affected by many factors such as the quality of the printing consumables, the mechanical transmission characteristics of the printer, and the print data generated by the slicing. In this paper, based on the actual needs, the printing accuracy, evaluation is carried out on the performance and control algorithm of the desktop level 3D printer designed in this paper. Comparison of the control algorithm put forward in this paper with the traditional algorithm shows that the proposed algorithm can reduce the time for establishing the topological relationship between the patches, which is simple to be implemented, stable and reliable.

6.1 Performance Test of the Embedded 3D Printer Prototype

(1) Model printing capacity, that is, whether a model can be printed out perfectly. The model printing capability is the basic requirement for the stability test of 3D printers. On the control pass, it mainly detects the anti-interference capacity of the printer and the sudden abnormal processing capability. For example, reading of print data, whether the mutual communication between modules in the printing process is stable, and effective processing of abnormal conditions. The test shows that the 3D printing control system designed in this paper can work continuously without failure under the condition of sufficient supplies. Figure 8 shows the diagram of the print molding effect. The comparison results suggest that the 3D printer model printing ability designed in this paper can complete the printing task and has relatively good stability.

Fig. 8. Model printing capability experiment

(2) Print dimensional accuracy. The so-called dimensional accuracy is the degree to which the actual size of the model fits the ideal size. The models for 3D printing are different. In this paper, the transverse dimensions of the model to be printed are experimentally compared, and the size of the circular axis and circular hole of the molded object is examined. Figure 9 shows a picture of the experimental model; Table 1 shows dimensional accuracy experimental data gives a comparison of the actual size of the experimental model to the ideal dimension. Based on the analysis of the data in Table 1, the absolute error of the inner diameter and the outer diameter of the model is within 0.2 mm in general. In addition, the relative error of the model with an outer diameter of 5 mm or more and an inner diameter of 10 mm or more can be controlled to be less than 1%.

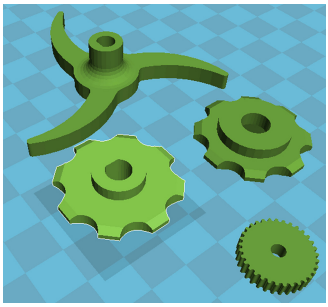

Fig. 9. Diagram of the experimental model

Table 1. Dimensional accuracy test data

	Outer diameter (mm)						Inner diameter (mm)					
Ideal value	50	40	30	20	10	5	40	30	20	10	5	3
First measurement	49.73	39.34	29.87	20.2	10.04	3.17	49.73	39.94	29.87	20.2	10.04	3.17
Second measurement	49.76	39.85	29.82	20.4	10.07	5.32	39.86	29.72	19.96	9.72	4.84	2.75
Third measurement	49.93	39.83	29.77	20	9.88	5.22	39.86	29.83	19.47	9.87	4.83	2.85
Fourth measurement	49.9	39.96	29.85	19.96	9.94	5.3	39.81	29.66	19.81	9.86	4.78	2.82
Fifth measurement	49.81	39.82	29.89	20.1	9.96	5.22	39.82	29.97	19.86	9.84	4.7	2.73
Mean value	49.82	39.88	29.84	20.13	9.97	5.25	39.81	29.83	19.9	9.85	4.80	2.81
Absolute value	0.175	0.12	0.159	0.132	0.022	0.246	0.186	0.166	0.1	0.152	0.198	0.192
Relative error	0.35%	0.30%	0.53%	0.66%	0.22%	4.92%	0.47%	0.55%	0.50%	1.52%	3.96%	6.40%

6.2 Embedded 3D Printer Control Algorithm Test

The embedded 3D printing manufacturing method based on the high elastomeric strain wireless sensor put forward in this paper is compared with two commonly used methods, that is, the classification method of the geometric features based on the STL model and the stratification method of the topology information based on the STL model. In the experiment of this paper, the two methods are referred to as Method 1 and Method 2, respectively.

In the experiment, the methods are evaluated from three aspects: the model stratification time, the memory space and the volume error. The three methods are applied to six models with different degrees of complexity. The STL model is shown in Fig. 10 as the following. The six models are numbered as model 1–6 in turn, and the number of triangle patches included in each model is shown in Table 1 as the following. The experimental environment is OpenGL and C++ is used as the language of the method. Table 2 lists the model stratification time, the memory space and the volume error obtained by the three methods for the six experimental models when the model stratification thickness is 0.01 mm. Due to the different complexity of the models, the differences in the experimental values at various angles are also relatively large, as shown in the following.

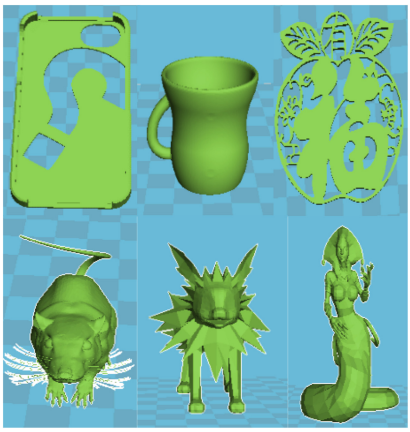

Fig. 10. Six STL models

Table 2. Results of the 6 models under 3 methods

	Model		Stratification time/s			Volume error/mm^3		
No.	Description	Number of batches	Method 1	Method 2	Method put forward in this paper	Method 1	Method 2	Method put forward in this paper
1	Mobile phone	961	1	0.89	0.32	65.83	65.79	65.43
2	Teacup	1244	1.25	1.13	0.56	0.25	0.24	0.23
3	Character	1942	2.1	1.93	1.12	39.46	39.35	39.30
4	Mouse	9960	10.01	8.89	3.60	22.24	22.35	22.18
5	Lion	19358	12.4	11.7	5.51	0.72	0.65	0.66
6	Cassiopeia	23826	21.43	20.9	10.32	18.35	18.29	18.36

The method put forward in this paper has obvious advantages in the aspect of the stratification operation efficiency. In addition, the time consumption relative to Method 1 and 2 is also greatly reduced, which is only about 18% of Method 2. For some STL models with the simple structure, the method put forward in this paper takes only tens or even hundreds of milliseconds. For the models with the number of patches up to 2×10^4, it takes only a dozen seconds. Hence, the applicability is relatively strong. In comparison, Method 1 is more applicable to the models with the simple structure. However, for the STL models with the number of triangle patches above 2×10^3, the time required for stratification increases and the method cannot be applied. Compared with Method 1, the stratification time of Method 2 is slightly reduced, but the process of establishing the topology data is highly time consuming and takes up a relatively large memory. For the models with the number of patches below 2×10^4, the stratification can be quickly completed within 20 s. However, for the models with highly complexity, it takes a long time to complete the stratification.

Figure 11 shows the comparison of the method put forward in this paper, Method 1, and Method 2 in reducing the volume deviation. Compared with Method 1, the method put forward in this paper can reduce the volume deviation by about 3.6% on average, which can even achieve about 7% compared with Models 2 and 5. However, there is slight fluctuation in the processing of Model 10. Compared with Method 2, the method put forward in this paper can reduce the volume deviation by about 1.16% on average, except for the individual model (Model 6). The magnitude of the decline is relatively small, which is only about 0.69%. The experimental results are within the expected range. Although the volume deviation becomes larger, the stratification efficiency has been significantly improved, as shown in the following.

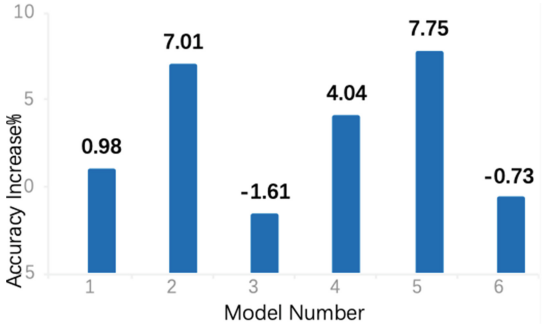

(a) Comparison with Method 1

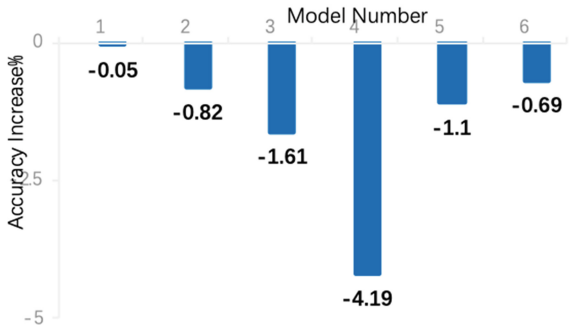

(b) Comparison with Method 2

Fig. 11. Comparison of the accuracy performance of different methods

7 Conclusions

With the continuous deepening of the 3D printing technology and applications, embedded 3D printer manufacturing has become a hot issue. In this paper, preliminary study is carried out on this issue. In view of the problem in the embedded 3D printer

manufacturing, a kind of embedded 3D printer manufacturing framework based on the high elastomeric strain wireless sensor is put forward. The design method can be used to implement the embedded 3D printer manufacturing with very little manual intervention. In addition, the framework can be extended to the shape manufacturing of other embedded 3D printing products.

References

1. Muth, J.T., Vogt, D.M., Truby, R.L.: Embedded 3D printing of strain sensors within highly stretchable elastomers. Adv. Mater. **26**(36), 6307–6312 (2014)
2. Li, F., Smejkal, P., Macdonald, N.P., Guijt, R.M., Breadmore, M.C.: One-step fabrication of a microfluidic device with an integrated membrane and embedded reagents by multimaterial 3D printing. Anal. Chem. **89**(8), 4701–4707 (2017)
3. Sun, K., Wei, T.S., Ahn, B.Y., Seo, J.Y., Dillon, S.J., Lewis, J.A.: 3D printing of interdigitated Li-ion microbattery architectures. Adv. Mater. **25**(33), 4539–4543 (2013)
4. Ladd, C., So, J.H., Muth, J., Dickey, M.D.: 3D printing of free standing liquid metal microstructures. Adv. Mater. **25**(36), 5081–5085 (2013)
5. Gebler, M., Schoot Uiterkamp, A.J.M., Visser, C.: A global sustainability perspective on 3D printing technologies. Energy Policy **74**, 158–167 (2014)
6. Fantino, E., Chiappone, A., Roppolo, I., Manfredi, D., Bongiovanni, R., Pirri, C.F., et al.: 3D printing: 3D printing of conductive complex structures with in situ generation of silver nanoparticles. Adv. Mater. **28**(19), 3711–3712 (2016)
7. Abbadessa, A., Blokzijl, M.M., Mouser, V.H.M., Marica, P., Malda, J., Hennink, W.E., et al.: A thermo-responsive and photo-polymerizable chondroitin sulfate-based hydrogel for 3D printing applications. Carbohydr. Polym. **149**, 163–174 (2016)
8. Spackman, C.C., Frank, C.R., Picha, K.C., Samuel, J.: 3D printing of fiber-reinforced soft composites: process study and material characterization. J. Manuf. Process. **23**, 296–305 (2016)
9. Parekh, D.P., Ladd, C., Panich, L., Moussa, K., Dickey, M.D.: 3D printing of liquid metals as fugitive inks for fabrication of 3D microfluidic channels. Lab Chip **16**(10), 1812–1820 (2016)
10. Castro, N.J., Patel, R., Zhang, L.G.: Design of a novel 3D printed bioactive nanocomposite scaffold for improved osteochondral regeneration. Cell. Mol. Bioeng. **8**(3), 416–432 (2015)
11. Javan, R., Zeman, M.N.: A prototype educational model for hepatobiliary interventions: unveiling the role of graphic designers in medical 3D printing. J. Digit. Imaging **31**(9), 1–11 (2017)
12. Pragnya, K., Keerti, K.: 3D printing high density ceramics using binder jetting with nanoparticle densifiers. Mater. Des. **155**, 443–450 (2018)
13. Gross, B., Lockwood, S.Y., Spence, D.M.: Recent advances in analytical chemistry by 3D printing. Anal. Chem. **89**(1), 57–70 (2017)
14. Zhang, B., Pei, X., Zhou, C., Fan, Y., Jiang, Q., Ronca, A., et al.: The biomimetic design and 3D printing of customized mechanical properties porous Ti6Al4V scaffold for load-bearing bone reconstruction. Mater. Des. **152**, 30–39 (2018)